Computers and Concrete, *Vol. 38, No. 1 (2026) 47-62*
https://doi.org/10.12989/cac.2026.38.1.047

Techno-Press

Sub-region retrieval based point-volume-element method for constructing concrete mesostructures with aggregate interference control

P. Guo, H.Y. Chen, L.J. Tu*, L.F. Fan

College of Architecture and Civil Engineering, Beijing University of Technology, Beijing, 100124, China

(Received April 15, 2026, Revised May 30, 2026, Accepted May 30, 2026)

Abstract. This paper proposed a numerical modeling method for constructing concrete model through the point-volume-element aggregate interference discrimination method based on sub-region retrieval. Firstly, the conventional concrete modeling method was enhanced by optimizing the interference discrimination logic between aggregates and the aggregate retrieval approach. Subsequently, a series of concrete models with varied aggregate geometric shapes, interfacial transition zone (ITZ) thicknesses, aggregate volume fractions, and aggregate gradations were generated, validating the reliability of the proposed method. Finally, the efficiency of the proposed method was validated by comparing the number of iterations and modeling time required with those of the conventional method. The results indicate that the proposed method can control the aggregate geometric shape and ITZ thickness by adjusting the number of vertices and the scaling distance. Compared to the conventional method, the proposed method significantly reduced the number of iterations and modeling time, thereby enhancing modeling efficiency. The advantage of the proposed method became more pronounced as the number of aggregates increased. When the number of generated aggregates reaches 100, the required number of iterations is reduced by 83.6%, and the modeling time is reduced by 66.2%.

Keywords: aggregate packing algorithm; aggregate shape control; computational efficiency; interfacial transition zone (ITZ); mesoscale concrete modeling

1. Introduction

Concrete is one of the most widely used construction materials, whose performance directly determines the safety and durability of structures [1-4]. The macroscopic mechanical performance of concrete is closely related to its complex internal structure, which primarily consists of aggregates, mortar matrix, and their interfacial transition zones (ITZ) [5-7]. Due to the complex internal structure of concrete, the investigation of its failure mechanisms, such as crack initiation and propagation, must be conducted at a meso-scale capable of characterizing the structural features of these components [8, 9]. Therefore, developing mesoscopic numerical models capable of accurately characterizing this heterogeneous internal structure of concrete is crucial for analyzing and predicting its mechanical performance [10-12].

In previous research, the numerical analysis of concrete primarily treated the material as an

*Corresponding author, Ph.D., E-mail: tulengjie@emails.bjut.edu.cn

http://www.techno-press.org/cac/5

ISSN: 1598-8198 (Print), 1598-818X (Online)

equivalent homogeneous continuum to analyze its macroscopic mechanical performance [13,14]. This geometrically homogeneous concrete model relies primarily on its own material constitutive model in numerical simulation, such as plastic damage models, fracture mechanics-based models, and crack propagation models [15, 16]. These constitutive models are further simulated using the finite element method to analyze the mechanical response of concrete under various loads [17]. On the one hand, through calibration with experimental data, homogeneous models have been able to capture certain typical characteristics of concrete mechanical behavior, including nonlinearity, strain softening, and post-peak ductility [18]. On the other hand, such homogeneous models also enable the analysis of overall concrete structures. These models have been successfully used to predict the load-bearing capacity, deformation behavior, and failure modes of reinforced concrete beams, columns, and slabs. The specific external loading conditions include static, dynamic, and cyclic loading [19, 20]. Furthermore, the homogeneous models have been extended to analyze complex mechanical behaviors such as creep, shrinkage, and thermal stress by incorporating time-dependent behavior and thermo-hygral coupling laws [21]. Currently, equivalent homogeneous models have demonstrated their capability to simulate and analyze the mechanical behavior of large-scale concrete structures, offering advantages in computational efficiency. The principle of those models fundamentally relies on a critical assumption. This assumption states that material heterogeneity can be sufficiently characterized by averaged homogeneous properties [22]. However, some studies have revealed that this assumption has inherent limitations under specific conditions. The fracture behavior, stress concentration, and size effects observed in actual experiments often cannot be fully explained or accurately predicted by homogeneous models alone [23-25]. Such models inherently smooth over localized stress concentrations and preferential crack paths, which are influenced by the heterogeneous mesoscopic structure of concrete. The discrepancies between homogenized simulation results and physical test data indicate that the internal heterogeneity of concrete is not merely a minor characteristic, but rather a critical factor affecting the mechanical behavior [26-28]. Based on this, it motivated the need for numerical modeling techniques of concrete that transcend the homogeneous continuum assumption [29-31].

To directly account for the influence of internal heterogeneity on concrete mechanical performance, extensive research has been devoted to developing and exploring mesoscopic modeling techniques that explicitly capture its multi-phase composition. Generally, concrete mesoscopic models typically treat concrete as a three-phase composite material [32]. Aggregates are randomly distributed within the mortar matrix and are interconnected through an ITZ with distinct properties. The ITZ is a thin region that closely surrounds each aggregate [33-35]. The core of these mesoscopic models is the algorithm for generating random aggregate structures, which must satisfy preset grading curves, aggregate volume fractions, and geometric constraints, such as minimum spacing [36]. Currently, many studies have proposed various algorithms for randomly generating aggregates. Aggregate generation algorithms have evolved from sequential placement approaches of simple spherical aggregates to advanced approaches. These advanced approaches can generate irregular polyhedral aggregates that better approximate the morphology of crushed stones [37, 38]. Based on this, the mesoscopic models deliver simulation fidelity that is unattainable with homogeneous models. These models have been used to simulate the complex fracture process of concrete. They reveal that cracks initiate within the weakened ITZ and then propagate by bypassing or penetrating aggregates within the mortar matrix, ultimately forming a macroscopic fracture surface [39]. Furthermore, the mesoscopic models have also been used to elucidate the mechanisms behind the dynamic strength enhancement of concrete, the influence of aggregate shape and distribution on mechanical performance, as well as the transport processes of chloride ions or sulfates within the concrete pore structure [40, 41]. The primary computational bottleneck in these mesoscopic modeling techniques is interference discrimination between aggregates, ensuring newly generated aggregates do not overlap with any existing ones [42]. The fundamental method for aggregate interference discrimination typically involves direct geometric detection of the aggregate shapes. Some studies have focused on improving detection efficiency through spatial management techniques, such as using background grid elements to localize neighbourhood searches or employing advanced data structures [43, 44]. Despite the significant advantages of three-dimensional mesoscopic models, their practical application remains constrained by low modeling efficiency. This limitation is particularly pronounced for the concrete model with aggregate volume fractions exceeding 40% [45]. As the aggregate volume fraction increases, the probability of successfully generating a new aggregate without interference decreases. Moreover, the number of attempts required to generate the aggregate and the associated geometric checks increases exponentially within the algorithm. This results in a time-consuming process for generating high-fidelity concrete mesoscopic models with high aggregate volume fractions. It limits the computational efficiency of numerical simulations for concrete models and restricts the application of mesoscale analysis to larger structural components [46-49]. Therefore, enhancing the efficiency of interference discrimination between aggregates not only represents an advancement in methods for concrete models but is also crucial for promoting the practical application of mesoscopic models in numerical studies of concrete [50-54].

In this study, a numerical method for constructing concrete mesoscopic models with high aggregate volume fractions was proposed, which achieves high computational efficiency through modified retrieval and interference discrimination approaches. The core modifications primarily involve the aggregate sub-region retrieval and point-volume-element aggregate interference discrimination. The efficiency of the proposed method was validated by comparing the number of iterations and modeling time required with those of the conventional method.

2. Method for constructing concrete mesoscopic numerical model

2.1 Mesoscopic structure of concrete

As a highly heterogeneous material, concrete consists of three distinct phases, which are coarse aggregate particles, the surrounding mortar matrix, and the ITZ that binds them together. Fig. 1

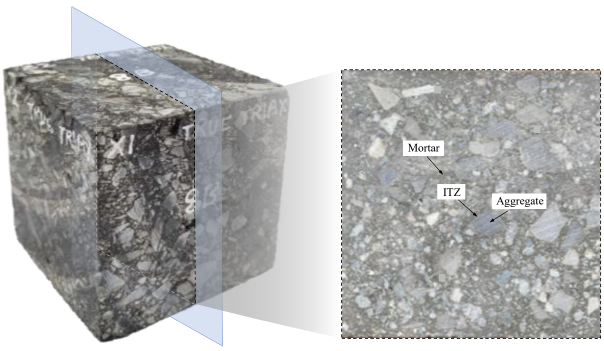

Figure 1. Mesoscopic structure of concrete (after Kumar et al. [55], and Lu et al. [56])

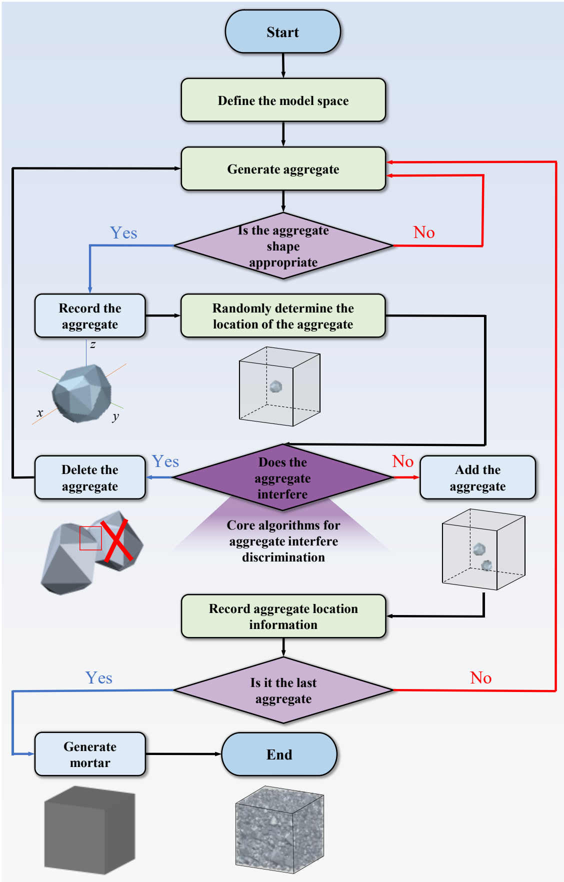

Figure 2. Flowchart for constructing the concrete numerical model

illustrates the fundamental mesoscale composition of concrete. At this mesoscale, concrete functions as a composite where the aggregates characterized by random shapes, sizes, and spatial distributions, serve as the primary stiff inclusions. These aggregates are embedded within the mortar matrix and exhibit a randomly distributed characteristic throughout the mortar matrix. The ITZ is a thin and microscopically porous region encircling each aggregate, which forms due to water accumulation and differential packing during hydration. This region typically exhibits higher porosity and weaker mechanical performance compared to the mortar, making it the primary pathway for microcrack initiation and propagation under stress. The macroscopic mechanical behavior of concrete, including its strength and fracture patterns, is fundamentally determined by the properties, volume fractions, and complex interactions of these three constituent phases. Therefore, constructing a mesoscopic numerical model of concrete must precisely capture the critical structural characteristics of these three constituent phases within concrete.

2.2 Modeling procedure

A method for constructing concrete mesoscopic models that precisely capture the internal structural characteristics is proposed, which offers higher modeling efficiency. Fig. 2 illustrates the algorithmic flowchart for constructing the concrete mesoscopic numerical model proposed in this paper. The modeling procedure begins with the definition of the geometric space of the target model, followed by the core stage of sequentially generating and placing coarse aggregates. For each aggregate, its shape and size are determined based on the type of predefined polyhedral geometric morphology and particle size. Subsequently, aggregates with geometrically unreasonable shapes are filtered out through a shape validity check. A candidate location for the aggregate is randomly determined within the model space, and interference discrimination is performed on the newly generated candidate aggregates. This includes the core algorithm for aggregate interference discrimination in numerical methods. The core of the proposed method lies in optimizing the interference discrimination process for aggregates. It abandons the global interference discrimination, which consumes substantial computational resources by checking against all placed aggregates. Instead, this method adopts a sub-region retrieval strategy combined with a multi-level discrimination logic. This allows for rapid and efficient retrieval of only those existing aggregates in the vicinity of the candidate location that could potentially cause overlap, and quickly determines whether interference occurs. If interference is detected, the polyhedral aggregate will not be placed, and a new candidate location will be attempted. This process iterates cyclically until a non-interfering location is found, at which point the aggregate is successfully added to the model, and its information is recorded. This cycle repeats until the target aggregate volume fraction is achieved. The remaining space not occupied by aggregates is filled with mortar matrix and ITZ, thereby completing the generation of the concrete mesoscopic numerical model. This optimized aggregate generation algorithm, which is centered on sub-region retrieval and multi-level interference discrimination, significantly reduces computational cyclic iterations.

The generation and placement of aggregates is the core stage in constructing the mesoscopic numerical model of concrete. Fig. 3 visually illustrates the sequential generation and placement of aggregates with different shapes and sizes within the model space, providing an intuitive overview of the entire procedure. This procedure initiates from a predefined aggregate library, which contains pre-generated aggregates with specific morphological characteristics. Individual aggregates are sequentially generated from this aggregate library and placed into the model space. Each newly generated aggregate is subjected to an interference discrimination check against nearby previously placed ones. This ensures that no spatial overlap occurs. The non-interfering

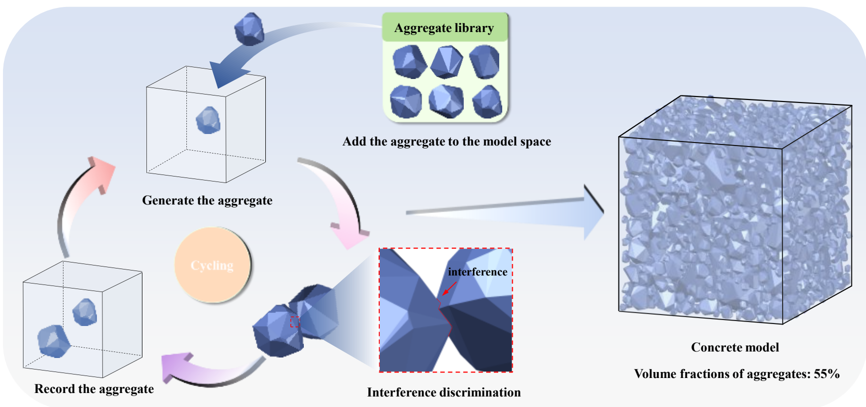

Figure 3. Aggregate placement process in concrete numerical models

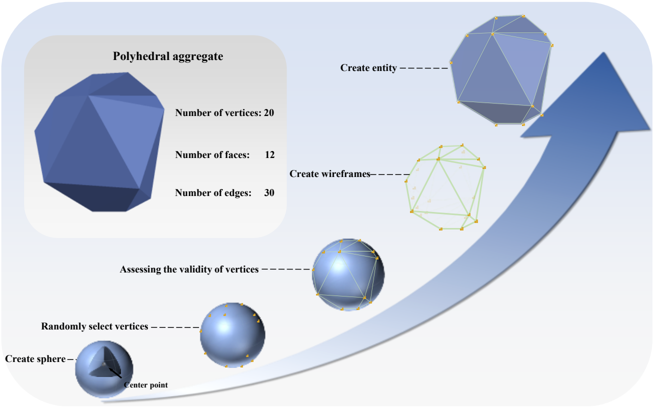

Figure 4. Generation and control of the polyhedral aggregate

aggregates are successfully placed into the model, and their spatial information is recorded. The iterative cycle of generation, interference discrimination, and placement continues until the target aggregate volume fraction is reached. Through this procedure, the aggregates are randomly distributed within the mesoscopic model. Moreover, as a critical model parameter, the aggregate volume fraction can be precisely controlled.

3. Core algorithms for control and discrimination in numerical models

Throughout the entire modeling procedure of aggregate generation and placement, several core control and discrimination algorithms are employed. These include the geometric shape control of aggregates and the ITZ, and the spatial interference discrimination of aggregates.

3.1 Geometric shape control of aggregates and ITZ

In the algorithm for the geometric shape control of aggregates and ITZ, this algorithm can produce more realistic polyhedral aggregates compared to simple spherical aggregates, which better approximate the angular characteristics of coarse aggregates. Fig. 4 illustrates the procedure for generating the polyhedral aggregate and controlling its morphology. The generation procedure begins by creating the sphere with a specified diameter. Its diameter corresponds to the target particle size of the aggregate, and the center point serves as the geometric center of the aggregate. Points are randomly selected on the surface of sphere to serve as the vertices for the polyhedral aggregate. Every point on the sphere surface has an equal probability of being selected. A validity assessment of the selected vertices is conducted to ensure the geometric stability of the generated aggregate and to avoid degenerate shapes, such as those with excessively sharp edges. Specifically, the distance between any two vertices should not be less than a prescribed threshold. If a vertex fails to meet this condition, the vertex selection process is repeated. Then, the polyhedral wireframe is created based on the selected vertices. The polyhedral wireframe is ultimately converted into an entity, which serves as the polyhedral aggregate. In this procedure, the algorithm controls the particle size of aggregates by adjusting the sphere diameter. The numbers of vertices, faces, and edges for aggregates are altered by adjusting the number of random points on

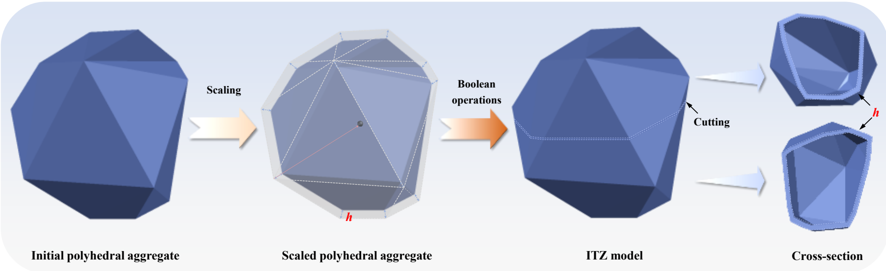

Figure 5. Generation and control of the ITZ

the surface of sphere. This enables precise control over the morphology of aggregates, providing a library of realistically shaped aggregates for subsequent placement.

In the algorithm for the generation and morphological control of ITZ, interfaces with controllable thickness that separate the aggregate from the mortar matrix can be generated separately for aggregates with different geometric morphologies. Fig. 5 illustrates the procedure for generating the ITZ and controlling its morphology. The generation procedure begins with the previously generated polyhedral aggregate, which has been created as an entity. For any initial polyhedral aggregate with different geometric morphology, each aggregate is uniformly scaled. Each vertex of the polyhedral is expanded outward along the direction from the geometric center by a specified thickness, which is defined as the ITZ thickness. This forms a scaled polyhedron that concentrically encloses the initial polyhedral aggregate. The ITZ is obtained by performing a Boolean subtraction operation on the scaled polyhedron, which removes the internal initial polyhedral aggregate. This operation removes the internal initial polyhedral aggregate, forming a hollow, shell entity that conforms to the surface morphology of the aggregate, which is the ITZ. The cross-section visually confirms that a uniform and continuous ITZ envelops the aggregate. The ITZ thickness is precisely controlled by the scaling distance parameter, ensuring the accuracy of the geometric morphology.

3.2 Spatial interference discrimination of aggregates

With the algorithms for generating and controlling aggregate and ITZ geometries established, the efficient spatial placement of these non-overlapping components within the model becomes critical. The proposed sub-region interference discrimination algorithm optimizes conventional aggregate interference discrimination methods by enhancing discrimination logic and retrieval approach. Fig. 6 illustrates the sub-region retrieval method, which substantially reduces the number of necessary retrievals through spatial partitioning. The principle of this algorithm lies in dividing the entire model space into uniformly sized small sub-regions. Each placed aggregate is registered to the specific sub-region it occupies based on its geometric center and shape. When placing a new candidate aggregate, the sub-region it will occupy is first identified. Only aggregates within this identified sub-region are retrieved for subsequent interference discrimination, rather than retrieving all previously placed aggregates. For instance, in case 1, a newly placed aggregate 1 is entirely located within a single region, such as region 3. Only the aggregates registered within this sub-region, such as aggregate 2 and aggregate 3, need to be retrieved. Aggregates in region 1 or region 2 do not need to be retrieved, as the spatial division inherently ensures their spatial isolation. In case 2, the newly placed aggregate 1 spans multiple regions due to its geometric size,

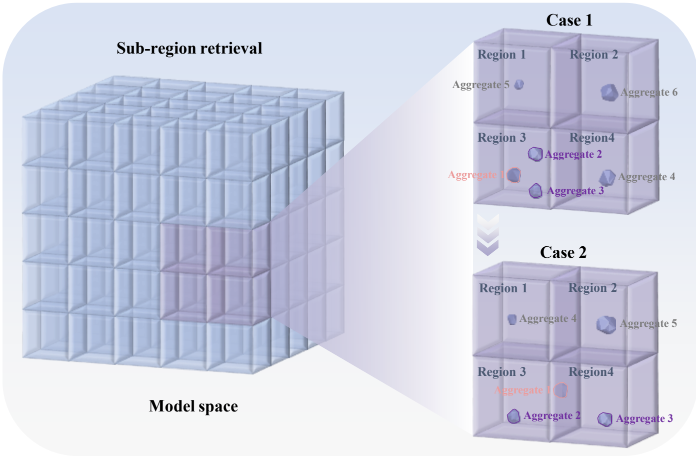

Figure 6. Sub-region retrieval aggregate method

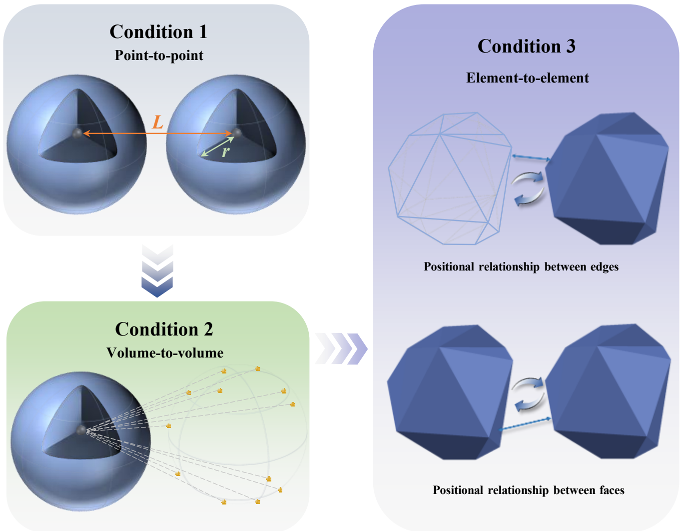

Figure 7. Point-volume-element aggregate interference discrimination method

such as occupying both region 3 and region 4. All aggregates registered within all the sub-regions it occupies must be retrieved, such as aggregate 2 and aggregate 3. This sub-region retrieval strategy transforms a global retrieval into a localized retrieval, thereby significantly reducing the number of subsequent interference discriminations.

Once the neighboring aggregates are retrieved through the sub-region retrieval method, a precise geometric check is required to confirm non-interference. Fig. 7 illustrates the point-volume-element interference discrimination method between aggregates, which employs a hierarchical logic for the interference check. The interference discrimination involves three sequentially discriminating conditions, forming a coarse-to-fine filtering mechanism. Condition 1 (point-to-point) performs a rapid discrimination between two polyhedral aggregates using their bounding spheres, which calculates the distance L between their geometric centers. If the distance L exceeds the sum of the radii of the bounding spheres, the aggregates are determined to be non-

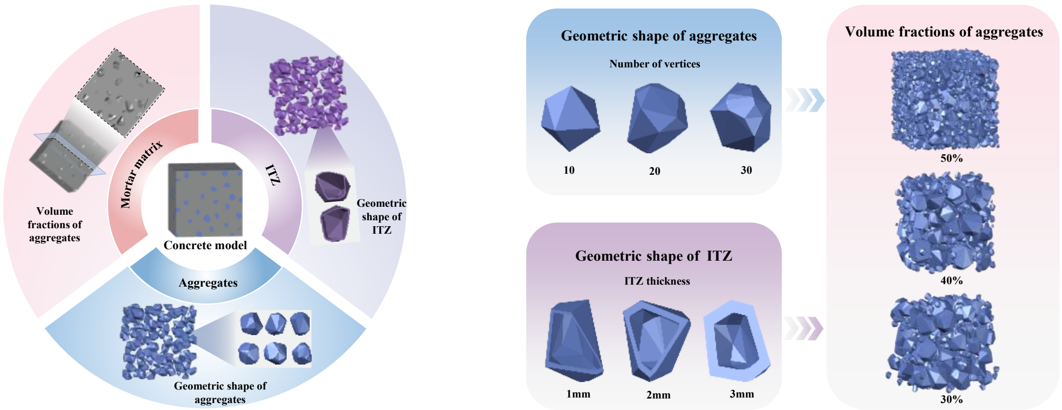

(a) Components of concrete numerical models (b) Parameter control of concrete numerical models

Figure 8. Concrete numerical models with different control parameters

interfering, and the discrimination terminates. This condition efficiently filters out clearly non-interfering aggregates. Otherwise, the process proceeds to condition 2 (volume-to-volume). This condition evaluates the spatial relationship between the vertices of the candidate aggregate and the bounding sphere of the existing aggregate. If all vertices of the candidate aggregate are located outside the bounding sphere of the existing aggregate, the aggregates are determined to be non-interfering, and the discrimination terminates. Finally, if both previous conditions are inconclusive, a more refined discrimination is executed. Condition 3 (element-to-element) evaluates the precise positional relationship between the two polyhedral elements, specifically checking for edge-to-edge and face-to-face interference between the polyhedral elements. This hierarchical discrimination strategy rapidly excludes clearly non-interfering aggregates through simple preliminary checks, reserving complex geometric calculations for only the necessary conditions, which significantly accelerates the overall discrimination process. Local retrieval and interference discrimination that progresses from simple to complex can reduce unnecessary computations while ensuring geometric accuracy.

4. Model application and validation

4.1 Model with different geometric morphology

Based on the core algorithm for multi-phase components generation and efficient aggregate interference discrimination, mesoscopic numerical models of concrete with different morphologies can be constructed. Fig. 8 presents a series of concrete mesoscopic numerical models, with geometric morphology controlled through parameters. As shown in Fig. 8(a), the concrete mesoscopic numerical model is clearly composed of coarse aggregates, the ITZ, and the mortar matrix that fills the remaining space. These components are mutually independent and exhibit no spatial interference. Fig. 8(b) presents the geometric morphology of concrete numerical models with different control parameters. The model control parameters include the number of polyhedral aggregate vertices, the ITZ thickness, and the aggregate volume fraction. Specifically, the geometric shape of the aggregates can be controlled by the number of vertices, enabling a

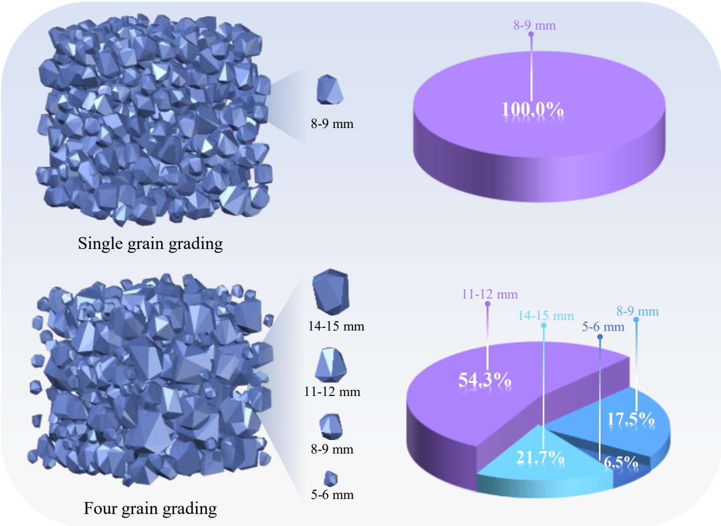

Figure 9. Concrete numerical models with different aggregate gradation

morphological transition from nearly spherical to highly angular polyhedra. Aggregates with different numbers of vertices exhibit distinct levels of surface complexity. The geometric shape of the ITZ can be precisely controlled by adjusting its thickness, enabling the generation of ITZ with specific thicknesses for aggregates of different shapes. Furthermore, the aggregate volume fraction within the model can be controlled by adjusting the number and size of placed aggregates. The comparison of models under different control parameter combinations confirms that the proposed method can generate concrete models with realistic mesoscopic structures.

In addition to the geometric shape of aggregates, ITZ thickness, and aggregates volume fraction, the gradation of aggregates is another critical characteristic of the concrete mesoscopic structure. Fig. 9 presents concrete mesoscopic numerical models with two different aggregate gradations. The first concrete mesoscopic model is generated using a single grain grading. All aggregates in this model have a particle size within the range of 8 mm-9 mm, accounting for 100%. The second concrete mesoscopic model is generated using a more realistic four grain grading, incorporating aggregates of four distinct particle sizes. The aggregate sizes include 5 mm-6 mm, 8 mm-9 mm, 11 mm-12 mm, and 14 mm-15 mm, which account for 6.5%, 17.5%, 21.7%, and 54.3% of the total aggregate volume, respectively. Comparing the two models reveals that the concrete mesoscopic model constructed with four grain grading exhibits greater heterogeneity. This indicates that the proposed aggregate generation and interference discrimination algorithms are not only applicable to single grain grading but are also capable of effectively placing aggregates with a predetermined size gradation. This capability is significant for practical concrete mesoscale modeling, where aggregate size distributions typically follow grading standards such as Fuller gradation.

4.2 Validation and comparison of modeling efficiency

The primary advantage of the proposed aggregate generation and interference discrimination algorithm lies in its high computational efficiency. Fig. 10 presents the comparison of modeling

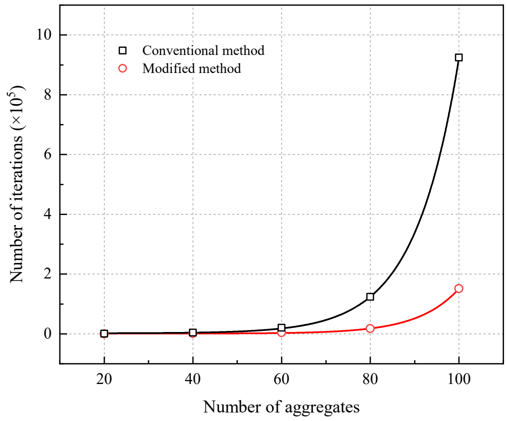

(a) Number of iterations

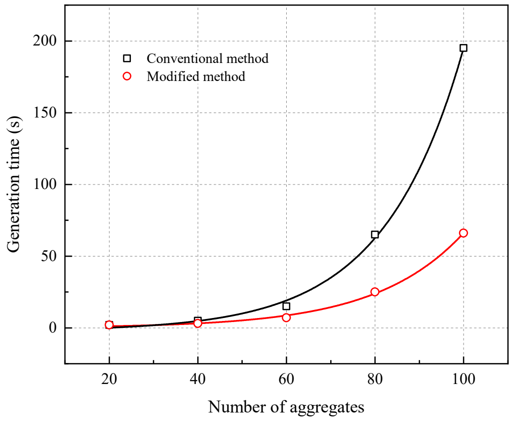

(b) Generation time

Figure 10. The comparison between the modified method and the conventional method

efficiency between the proposed method and the conventional method. Fig. 10(a) illustrates the relationship between the number of iterations required to generate the concrete model and the number of placed aggregates using the conventional method and the modified method. For the conventional method, the number of iterations increases exponentially as the number of aggregates increases. In contrast, for the modified method, while the number of iterations also increases exponentially with the number of aggregates, the increase is significantly more gradual. As the number of placed aggregates exceeds 60, the divergence in efficiency between the conventional method and the modified method gradually widens. For example, when the number of placed aggregates reaches 100, the modified method reduces the number of iterations by 83.6% compared to the conventional method. Fig. 10(b) illustrates the relationship between the modeling time required to generate the concrete model and the number of placed aggregates using the conventional method and the modified method. For the conventional method, the modeling time exhibits an exponential increase trend as the number of aggregates increases. In contrast, the modeling time for the modified method also increases with an increasing number of aggregates, but the rate of increase is substantially more gradual. This divergence in time consumption becomes progressively more pronounced as the number of placed aggregates exceeds 60. For example, when the number of placed aggregates reaches 100, the modified method reduces the modeling time by 66.2% compared to the conventional method. This consistent trend validates the exceptional efficiency of the modified method in generating complex concrete mesoscopic models. The proposed method provides a solid basis for simulating concrete structural components by significantly reducing computational costs. However, when applied to full-scale large concrete structures, such as large bridge piers or dams, further improvements in computational efficiency may still be required due to the significant increase in the number of aggregates and the size of the models.

The theoretical implication of this efficiency improvement is that it validates the effectiveness of local retrieval and hierarchical discrimination in the process of generating high-volume-fraction aggregates. Practically, the reduced modeling time enables more extensive parametric studies for concrete structures, thereby providing a scientific basis for material design and structural safety assessment.

5. Conclusions

This study proposed an efficient method for constructing the concrete mesoscopic model. The interference discrimination logic between aggregates and the aggregate retrieval was optimized. The reliability of the proposed method was validated by generating concrete models with different geometries and aggregate gradations. The enhanced efficiency of the proposed method was validated by comparing the modeling efficiency between the proposed method and the conventional method. The conclusions obtained are as follow:

(1) The proposed method optimizes the aggregate interference discrimination process through a sub-region retrieval strategy and a point-volume-element interference discrimination logic. The sub-region retrieval strategy transforms a global retrieval into a localized retrieval, while the point-volume-element discrimination logic rapidly excludes obviously non-interfering aggregates, reserving complex geometric calculations only for necessary conditions.

(2) The proposed method enables precise control of the aggregate geometric shape and ITZ thickness by adjusting the number of vertices and the scaling distance, respectively. Moreover, concrete mesoscopic models with different aggregate gradations can also be constructed by controlling the placement of aggregates.

(3) The proposed method significantly reduced the number of iterations and modeling time compared to the conventional method. This advantage of the proposed method became more pronounced as the number of aggregates increased. When the number of generated aggregates reaches 100, the required number of iterations is reduced by 83.6%, and the modeling time is reduced by 66.2%.

Conflict of interest

The authors declare that they have no conflict of interest.

Data availability

Data associated with this research are available and can be obtained by contacting the corresponding author.

References

1. Ummin, O., Li, Y., Li, K., Chen, Y.Y., Jia, H.Y., Zuo, J. (2024). Influence of surface roughness and interfacial agent on the interface bonding characteristics of polyurethane concrete and cement concrete. Journal of Building Engineering, 91, 109596. https://doi.org/10.1016/j.jobe.2024.109596.
2. Wu, Q.L., Xu, S.C., Wu, S.Y., Cai, X., Bu, R.F., Sun, X.F. (2024). Anti-clogging performance of pervious concrete incorporating hydrophobic agent. Construction and Building Materials, 431, 136554. https://doi.org/10.1016/j.conbuildmat.2024.136554.
3. Ding, X.H., Ma, T., Zhang, W.G., Zhang, D.Y., Yin, T. (2018). Effects by property homogeneity of aggregate skeleton on creep performance of asphalt concrete. Construction and Building Materials, 171, 205-213. https://doi.org/10.1016/j.conbuildmat.2018.03.150.
4. Shehadeh, A., Alshboul, O., Saleh, E. (2024). Enhancing safety and reliability in multistory

construction: A multi-state system assessment of shoring/reshoring operations using interval-valued belief functions. Reliability Engineering & System Safety, 252, 110458. https://doi.org/10.1016/j.ress.2024.110458.

5. Peng, Z.S., Xiong, Q.X., Zhou, X.M., Gao, X., Zhao, X.Y., Meng, Z.Z., Liu, Q.F. (2025). A porosity-based mechanics model for studying crack evolution from ITZ to mortar matrix in concrete. Computer Methods in Applied Mechanics and Engineering, 444, 118085. https://doi.org/10.1016/j.cma.2025.118085.
6. Qiu, J.S., Zhou, Y.X., Guan, X., Zhu, M.Y. (2021). The influence of fly ash content on ITZ microstructure of coal gangue concrete. Construction and Building Materials, 298, 123562. https://doi.org/10.1016/j.conbuildmat.2021.123562.
7. Wu, K., Shi, H.S., Xu, L.L., Ye, G., De Schutter, G. (2016). Microstructural characterization of ITZ in blended cement concretes and its relation to transport properties. Cement and Concrete Research, 79, 243-256. https://doi.org/10.1016/j.cemconres.2015.09.018.
8. Qi, X.P., Zhang, J., Rajeev, A., Liu, J., Wang, Z.Y., Liu, Z.F., Zhang, F.L., Wang, Z.H. (2024). Effect of coarse aggregates on contact explosion resistance of concrete-A mesoscopic investigation. Engineering Fracture Mechanics, 311, 110576. https://doi.org/10.1016/j.engfracmech.2024.110576.
9. Yao, Z.Y., Qin, F., Li, J.Z., Zhang, X.H., Huang, F.L. (2025). Experimental and 3D mesoscopic numerical simulation study of kinetic projectile penetrating into concrete. International Journal of Impact Engineering, 195, 105140. https://doi.org/10.1016/j.ijimpeng.2024.105140.
10. Wu, P., Deng, Y.Y., Ma, C.L., Wang, Z.H., Li, L.L., Zhang, Y.N. (2026). Perforation performance study and residual velocity prediction of reactive powder concrete based on mesoscopic numerical simulation and experiments. International Journal of Impact Engineering, 210, 105596. https://doi.org/10.1016/j.ijimpeng.2025.105596.
11. Feng, T.T., Wang, F.J., Tan, Y.S., Yue, C.J., Xu, W.X., Liu, Z.Y., Yang, Z.Q., Wu, Y.R., Jiang, J.Y. (2022). Dynamic compression mechanical properties of eco-friendly ultra-high performance concrete produced with aeolian sand: Experimental and three-dimensional mesoscopic investigation. International Journal of Impact Engineering, 164, 104192. https://doi.org/10.1016/j.ijimpeng.2022.104192.
12. Chen, F.J., Li, B., Li, D., Jin, L., Du, X.L. (2024). Bond stress-slip relationship of CFRP bar-concrete interface of CFRP reinforced concrete subjected to reversed cyclic loading. Engineering Structures, 314, 118231. https://doi.org/10.1016/j.engstruct.2024.118231.
13. Tang, B., Cui, W., Zhang, B.Z., Jiang, Z.A. (2023). The macroscopic mechanical characteristics and microscopic evolution mechanism of plastic concrete. Construction and Building Materials, 391, 131898. https://doi.org/10.1016/j.conbuildmat.2023.131898.
14. Unosson, M., Nilsson, L. (2006). Projectile penetration and perforation of high performance concrete: Experimental results and macroscopic modelling. International Journal of Impact Engineering, 32, 1068-1085. https://doi.org/10.1016/j.ijimpeng.2004.11.003.
15. Guo, W., Fan, W., Shao, X.D., Shen, D.J., Chen, B.S. (2018). Constitutive model of ultra-high-performance fiber-reinforced concrete for low-velocity impact simulations. Composite Structures, 185, 307-326. https://doi.org/10.1016/j.compstruct.2017.11.022.
16. Valentini, B., Theiner, Y., Aschaber, M., Lehar, H., Hofstetter, G. (2013). Single-phase and multi-phase modeling of concrete structures. Engineering Structures, 47, 25-34. https://doi.org/10.1016/j.engstruct.2012.04.039.
17. Tai, Y.S., Tang, C.C. (2006). Numerical simulation: The dynamic behavior of reinforced concrete plates under normal impact. Theoretical and Applied Fracture Mechanics, 45, 117-127. https://doi.org/10.1016/j.tafmec.2006.02.007.
18. Li, P.D., Wu, Y.F., Zhou, Y.W., Xing, F. (2018). Cyclic stress-strain model for FRP-confined concrete considering post-peak softening. Composite Structures, 201, 902-915. https://doi.org/10.1016/j.compstruct.2018.06.088.
19. Shi, Y.C., Lu, Y., Cui, J. (2024). Numerical study on dynamic shear properties of concrete under high loading rates. Engineering Failure Analysis, 163, 108569. https://doi.org/10.1016/j.engfailanal.2024.108

569.
20. Song, Z.Y., Konietzky, H., Herbst, M. (2019). Three-dimensional particle model based numerical simulation on multi-level compressive cyclic loading of concrete. Construction and Building Materials, 225, 661-677. https://doi.org/10.1016/j.conbuildmat.2019.07.260.
21. Wang, J.L., Yang, L.F., Huang, J.H., Yu, B. (2023). Service life prediction model for marine concrete structures considering structural shape and time-dependent behaviour. Ocean Engineering, 285, 115276. https://doi.org/10.1016/j.oceaneng.2023.115276.
22. Congro, M., Sanchez, E.C.M., Roehl, D., Marangon, E. (2019). Fracture modeling of fiber reinforced concrete in a multiscale approach. Composites Part B: Engineering, 174, 106958. https://doi.org/10.1016/j.compositesb.2019.106958.
23. Guan, Z.H., Li, Y., Lai, Z.C., Zhou, H., Qin, J., Wen, Y.B., Chen, Y.F., Huang, R.Y. (2024). Size effect of concrete based on split Hopkinson pressure bar (SHPB) test. Construction and Building Materials, 441, 137499. https://doi.org/10.1016/j.conbuildmat.2024.137499.
24. Shah, S.G., Kishen, J.M.C. (2010). Fracture behavior of concrete-concrete interface using acoustic emission technique. Engineering Fracture Mechanics, 77, 908-924. https://doi.org/10.1016/j.engfracmech.2010.01.018.
25. Schneider, U., Chen, S.W. (2005). Deterioration of high-performance concrete subjected to attack by the combination of ammonium nitrate solution and flexure stress. Cement and Concrete Research, 35, 1705-1713. https://doi.org/10.1016/j.cemconres.2004.11.011.
26. Yang, Z.J., Li, B.B., Wu, J.Y. (2019). X-ray computed tomography images based phase-field modeling of mesoscopic failure in concrete. Engineering Fracture Mechanics, 208, 151-170. https://doi.org/10.1016/j.engfracmech.2019.01.005.
27. Lin, Y.J., Zhong, S.Y., Jiang, S.H., Cheng, T.Y., Zhou, J. (2025). Mesoscopic simulation of the thermodynamic behavior of concrete-encased structural steel composites under freeze-thaw cycles. Computers and Structures, 319, 107971. https://doi.org/10.1016/j.compstruc.2025.107971.
28. Wu, H., Li, Y.C., Fang, Q., Peng, Y. (2019). Scaling effect of rigid projectile penetration into concrete target: 3D mesoscopic analyses. Construction and Building Materials, 208, 506-524. https://doi.org/10.1016/j.conbuildmat.2019.03.040.
29. Shehadeh, A., Alshboul, O. (2025). Enhancing engineering and architectural design through virtual reality and machine learning integration. Buildings, 15, 328. https://doi.org/10.3390/buildings15030328.
30. Shehadeh, A., Alshboul, O., Taamneh, M.M., Jaradat, A.Q., Alomari, A.H. (2024). Enhanced clash detection in building information modeling: Leveraging modified extreme gradient boosting for predictive analytics. Results in Engineering, 24, 103439. https://doi.org/10.1016/j.rineng.2024.103439.
31. Alshboul, O., Shehadeh, A., Almasabha, G. (2025). Reliability of information-theoretic displacement detection and risk classification for enhanced slope stability and safety at highway construction sites. Reliability Engineering & System Safety, 256, 110813. https://doi.org/10.1016/j.ress.2025.110813.
32. Li, K.Q., Li, D.Q., Liu, Y. (2020). Meso-scale investigations on the effective thermal conductivity of multi-phase materials using the finite element method. International Journal of Heat and Mass Transfer, 151, 119383. https://doi.org/10.1016/j.ijheatmasstransfer.2020.119383.
33. Su, Y.T., Iyela, P.M., Zhu, J.Q., Chao, X.J., Kang, S.B., Long, X. (2024). A Voronoi-based gaussian smoothing algorithm for efficiently generating RVEs of multi-phase composites with graded aggregates and random pores. Materials & Design, 244, 113159. https://doi.org/10.1016/j.matdes.2024.113159.
34. Peng, R.X., Qiu, W.L., Jiang, M. (2022). Micromechanical modeling of frozen concrete by micro-deformation of multi-phase composite material. Composite Structures, 301, 116224. https://doi.org/10.1016/j.compstruct.2022.116224.
35. Ma, G., Wang, F. (2024). A DEM-based framework to optimize the gradation of concrete aggregate using fractal approach. Computational Particle Mechanics, 11, 2203-2214. https://doi.org/10.1007/s40571-024-00774-3.
36. Zhou, X., Xie, Y.J., Long, G.C., Zeng, X.H., Li, J.T., Yao, L., Jiang, W.H., Pan, Z.L. (2021). DEM analysis of the effect of interface transition zone on dynamic splitting tensile behavior of high-strength concrete based on multi-phase model. Cement and Concrete Research, 149, 106577.

https://doi.org/10.1016/j.cemconres.2021.106577.
37. Liu, C., Xie, D.Q., She, W., Liu, Z.Y., Liu, G.J., Yang, L., Zhang, Y.S. (2018). Numerical modelling of elastic modulus and diffusion coefficient of concrete as a three-phase composite material. Construction and Building Materials, 189, 1251-1263. https://doi.org/10.1016/j.conbuildmat.2018.08.191.
38. Zeng, M.H., Wu, Z.M., Zheng, J.J., Yu, R.C. (2023). A mesoscopic numerical method for fracture energy of concrete. Fatigue & Fracture of Engineering Materials & Structures, 46, 2380-2395. https://doi.org/10.1111/ffe.14001.
39. Kim, J.Y., Park, H.G., Yi, S.T. (2011). Plasticity model for directional nonlocality by tension cracks in concrete planar members. Engineering Structures, 33, 1001-1012. https://doi.org/10.1016/j.engstruct.2010.12.023.
40. Hu, Y.Q., Hu, S.W., Ye, Y.X., Li, W.H., Li, C.Z. (2024). Time-varying analytical model and mesoscopic numerical simulation of chloride ion diffusion in prestressed concrete cylinder pipe. Journal of Building Engineering, 94, 109951. https://doi.org/10.1016/j.jobe.2024.109951.
41. Xu, X.B., Zheng, Y.L., Hou, C.Y., Lan, X., Pan, T.B., Zhang, Z.X. (2025). Investigation of chloride ion diffusion mechanism and durability analysis of offshore concrete structures under fatigue loading. Engineering Fracture Mechanics, 317, 110942. https://doi.org/10.1016/j.engfracmech.2025.110942.
42. Quan, W.W., Ma, X.Y., Li, X.K., Dong, Z.J. (2022). Efficient numerical model for effective thermal conductivity of concrete with aggregates of different morphologies and imperfect interfaces. International Journal of Heat and Mass Transfer, 185, 122358. https://doi.org/10.1016/j.ijheatmasstransfer.2021.122358.
43. Yu, P., Ren, Z.Y., Chen, Z., Bordas, S.P.A. (2023). A multiscale finite element model for prediction of tensile strength of concrete. Finite Elements in Analysis and Design, 215, 103877. https://doi.org/10.1016/j.finel.2022.103877.
44. Ouyang, H., Chen, X.W. (2020). 3D meso-scale modeling of concrete with a local background grid method. Construction and Building Materials, 257, 119382. https://doi.org/10.1016/j.conbuildmat.2020.119382.
45. Gangnant, A., Saliba, J., La Borderie, C., Morel, S. (2016). Modeling of the quasibrittle fracture of concrete at meso-scale: Effect of classes of aggregates on global and local behavior. Cement and Concrete Research, 89, 35-44. https://doi.org/10.1016/j.cemconres.2016.07.010.
46. Qin, X.N., Gu, C.S., Shao, C.F., Fu, X., Vallejo, L., Chen, Y. (2020). Numerical analysis of fracturing behavior in fully-graded concrete with oversized aggregates from mesoscopic perspective. Construction and Building Materials, 253, 119184. https://doi.org/10.1016/j.conbuildmat.2020.119184.
47. Bai, F.T., Li, Y.S., Liu, L.B., Li, X.M., Liu, W.X. (2023). An efficient and high-volume fraction 3D mesoscale modeling framework for concrete and cementitious composite materials. Composite Structures, 325, 117576. https://doi.org/10.1016/j.compstruct.2023.117576.
48. Fan, L.F., Yang, Q.H., Du, X.L. (2024). Spalling characteristics of high-temperature treated granitic rock at different strain rates. Journal of Rock Mechanics and Geotechnical Engineering, 16, 1280-1288. https://doi.org/10.1016/j.jrmge.2023.05.016.
49. Yang, Q.H., Fan, L.F., Du, X.L. (2026). Predicting the storage modulus of granite after high-temperature exposure. Journal of Rock Mechanics and Geotechnical Engineering. https://doi.org/10.1016/j.jrmge.2025.12.021.
50. Shehadeh, A., Alshboul, O., Taamneh, M.M., Jaradat, A.Q., Alomari, A.H., Arar, M. (2025). Advanced integration of BIM and VR in the built environment: Enhancing sustainability and resilience in urban development. Heliyon, 11, e42558. https://doi.org/10.1016/j.heliyon.2025.e42558.
51. Alshboul, O., Shehadeh, A. (2026). Enhancing infrastructure project outcomes through optimized contractual structures and long-term warranties. Engineering, Construction and Architectural Management, 33, 2220-2242. https://doi.org/10.1108/ECAM-07-2024-0954.
52. Alshboul, O., Shehadeh, A., Saleh, E. (2025). Advancing construction quality management: An integrated evidential reasoning and belief functions framework. Journal of Construction Engineering and Management, 151(8), 04025093. https://doi.org/10.1061/JCEMD4.COENG-15969.
53. Fan, L.F., Duan, X.L., Yang, Q.H., Du, X.L. (2026). A unified series solution for SH-wave scattering by

a bisymmetric triangular combined terrain. Applied Mathematical Modelling, 156, 116885. https://doi.org/10.1016/j.apm.2026.116885.

54. Duan, X.L., Fan, L.F., Zhou, Z.H., Du, X.L. (2026). A unified analytical solution for seismic response of a symmetrical triangular hill or canyon subjected to SH waves. International Journal for Numerical and Analytical Methods in Geomechanics, 50, 558-578. https://doi.org/10.1002/nag.70114.
55. Kumar, A., Serati, M., Van Wijk, I., Vangla, P., Ramana, G.V. (2025). True triaxial behaviour and failure criteria of asphalt mixes with crushed waste glass fine aggregates. Construction and Building Materials, 500, 144106. https://doi.org/10.1016/j.conbuildmat.2025.144106.
56. Lu, Y., Shi, Y.C., Cui, J. (2025). Experimental study on multiaxial tensile behaviors of concrete. Construction and Building Materials, 487, 141975. https://doi.org/10.1016/j.conbuildmat.2025.141975.